RSC Advances

PAPER

View Article Online
View Journal | View Issue

Cite this: *RSC Adv.*, 2020, **10**, 28935

Early osteoblastic activity on TiO_2 thin films decorated with flower-like hierarchical Au structures

Spyridon Kalantzis,†[a] Salih Veziroglu, †[b] Theresa Kohlhaas,[a] Christian Flörke,[a] Yogendra Kumar Mishra,[c] Jörg Wiltfang,[a] Yahya Açil,[a] Franz Faupel,[b] Oral Cenk Aktas *[bd] and Aydin Gülses *[a]

Received 11th June 2020
Accepted 27th July 2020

DOI: 10.1039/d0ra05141a

rsc.li/rsc-advances

Titanium alloys are the most commonly used dental and orthopedic implant materials due to their proven biocompatibility and mechanical properties. The native oxide layer (TiO_2 layer) formed on such Ti-based implants acts as the self-protecting layer against possible ion release. Increasing the oxide layer thickness further on such TiO_2 implants even opens the triggering of the osseointegration process if the oxide layer is having a certain degree of roughness, preferably higher. This work reports a novel photocatalytic patterning of sputter deposited TiO_2 layers with flower-like Au structures to enhance the early osteoblastic activity. The prepared hierarchical Au structures, composed of micro- and nanoscale features on the top, lead to improved number of filopodia formation. This suggest that proposed Au–TiO_2 surface may foster the cell attachment and as well as cell proliferation.

1. Introduction

Titanium (Ti) and its alloys are the most commonly used dental and orthopedic implant materials due to their proven biocompatibility, mechanical properties, and non-toxicity.[1,2] Long-term performance of such implants depends on their initial stability and early osseointegration.[3,4] Cell adhesion to the implant surface, which is the first step in tissue-implant interaction, plays a major role on cell proliferation, differentiation, bone formation, and ultimate osseointegration.[5] Various studies showed both chemical and physical properties of the implant surface influence cellular response at the tissue-implant interface.[6,7] A native oxide layer (1–5 nm thick TiO_2 layer) formed on Ti-based implants is known to act as a barrier between the implant and tissue to prevent any possible ion release, thus this helps to suppress a strong immune response.[6] On the contrary, recent studies have indicated only a few-nanometer thick oxide layer on a typical Ti-based implant does not provide sufficient long-term chemical stability and thicker oxide layers are shown to accelerate the osteointegration.[8] Additionally, it has been reported that the physical topography and the structure of the TiO_2 layer on Ti-based implants (surface roughness, surface wettability, surface energy, surface phase, *etc.*) promotes cell adhesion and proliferation while minimizing bacterial colonization.[9,10]

Various methods including electron beam evaporation, sol–gel, electrospinning, pulsed laser deposition (PLD), chemical vapor deposition (CVD), atomic layer deposition (ALD) and sputtering have been proposed to prepare functional TiO_2 coatings for implants.[11,12] Among these methods, sputtering possesses several advantages in the deposition of TiO_2, such as strong bonding strength, excellent large-area uniformity, and proven reproducibility and straightforward scale-up.[13,14] By modifying sputtering process parameters such as sputtering power, substrate temperature, and incident deposition angle one can tailor the surface topography of the TiO_2 layer, which plays a critical role on cell–surface interaction.[15] On the other hand, this is limited to some typical morphologies including columnar and island type structures.[16] For the addition of micro- and nanostructured features on sputter-deposited TiO_2 layers mostly a secondary process such as gas-phase etching is needed. However, such energetic etching processes are known to result in damage and contamination in the film.[17]

Recently, we reported a novel photocatalytic patterning method to structure TiO_2 thin films. The method allows patterning of the TiO_2 surface with hierarchical Au micro- and nanostructures.[18] Due to their excellent biocompatibility and ease of modification with various functional groups, Au nanostructures have been used in various biomedical applications

[a]*Department of Oral and Maxillofacial Surgery, University Hospital of Schleswig-Holstein, Campus Kiel, Arnold-Heller-Straße 3, 24105 Kiel, Germany. E-mail: aguelses@mkg.uni-kiel.de*

[b]*Chair for Multicomponent Materials, Institute for Materials Science, Faculty of Engineering, Kiel University, Kaiserstr. 2, 24143 Kiel, Germany. E-mail: oca@tf.uni-kiel.de*

[c]*Mads Clausen Institute, NanoSYD, University of Southern Denmark, Alsion 2, 6400 Sønderborg, Denmark*

[d]*Department of Metallurgical and Materials Engineering, Faculty of Engineering, METU – Middle East Technical University, Çankaya, 06800 Ankara, Turkey*

† Both authors contributed equally.

including bio-sensing, diagnosis, intracellular imaging, and drug delivery.[19] Additionally, Au nanostructures act as a suitable platform for the investigation of the influence of surface topography on cell adhesion, proliferation, and differentiation.[20,21] Herein, we prepared flower-like hierarchical Au structures on a stable TiO_2 thin film for investigating early adhesion behavior of human osteoblasts (HOBs) to reveal their potential application in dental implants. The proposed method is not limited to only Au, various types of metals can be deposited on the TiO_2 surface to achieve hierarchical structures as well as additional functionalities.[22]

2. Materials and methods

2.1. Preparation of TiO_2 thin films

TiO_2 thin films were deposited on Ti substrates by using a custom-built pulsed DC reactive magnetron sputtering method from a metallic titanium target (Ti-Goodfellow, 99.99% with a 50 mm diameter) in the presence of oxygen (O_2, reactive gas) and argon (Ar, process gas).[23] First, substrates were cleaned in an ultrasonic bath by using acetone, isopropanol, and water respectively and subsequently dried with nitrogen (N_2) gas. Then, substrates were placed into the custom-made vacuum chamber and the base pressure was adjusted about 5×10^{-5} Pa. Ti target was cleaned for 10 min by pure Ar plasma at 250 sccm Ar flow. Subsequently, an O_2 flow of 10 sccm was injected into the vacuum chamber while DC power (90 W) operated at a frequency of 50 kHz with 55% duty cycle to reduce the excessive oxidation and the poisoning of the target surface. Substrates were rotated at 30 rpm during the sputtering to obtain a homogeneous film. The deposition time was kept around 3 hours to achieve a thickness of 900 nm. Afterward, deposited TiO_2 thin films were heat-treated in an oven (Nabertherm, LE 4/11/R6) at 650 °C for 60 min and afterward directly quenched in the air.

2.2. Photocatalytic deposition of Au clusters

Au clusters were deposited on the TiO_2 thin films by a slightly modified photocatalytic deposition method as schematically shown in Fig. 1.[18,24,25] The starting materials, gold(III) chloride ($AuCl_3$) was purchased from Alfa Aesar. The TiO_2 thin films were dipped into a quartz cuvette, filled with 6.5 ml of an aqueous $AuCl_3$ (0.8×10^{-3} M). Samples were illuminated by low-intensity UV light (4.5 mW cm^{-2}, UV lamp operating at $\lambda =$ 365 nm) for 10 minutes. After UV illumination, the samples were rinsed with deionized water and dried with air to remove any residual solution on the substrate.

2.3. Surface analysis

Scanning Electron Microscopy (SEM, Supra55VP-Carl Zeiss) was used to reveal the surface morphology of prepared samples. For static contact angle measurements, a semi-automated CA meter (OCA 30, Dataphysics) was performed. Here, 10 μL of water droplets were used and advancing/receding CAs were recorded and measured by the addition and subtraction of water to/from droplets sitting on the sample surface.

2.4. Cell culture

Human osteoblasts (HOBs) were isolated from patients who underwent oral surgical interventions in the Department of Oral and Maxillofacial Surgery at Christian Albrechts Universität zu Kiel. Briefly, jawbone tissues were mechanically removed from the specimens, cut into fragments of 0.3–0.5 cm in diameter and extensive washing in phosphate-buffered solution (pH: 7.4) was performed. The fragments were seeded as explants into the culture flasks and cultivated at 37 °C in a humidified atmosphere of 95% air and 5% CO_2. Culture medium was Dulbecco's Modified Eagle's Medium, supplemented with fetal calf serum, 10^5 penicillin, 100 mg L^{-1} streptomycin, 2 mM L-glutamine, 100 nM dexamethasone and 1 mM L-ascorbic acid 2-phosphatase (Sigma, Deisenhofen Germany). Cells were subcultures in a second passage at a density of 3.3×10^6 cm^{-2}. For the second passage, a cell dispenser was used to bring the cells into suspension. One hundred microliters containing 3.3×10^5 osteoblast-like cells in the second passage were transferred onto the matrix samples. All experiments were performed in triplicate and following the 12 and 24 hours of incubation.

2.5. Staining of cells

For the determination of the viable and necrotic cells, staining with fluorescein diacetate (FDA, Sigma-Aldrich, St. Louis, USA) and propidium iodide (PI, Sigma-Aldrich, St. Louis, USA) were used. Eight well plates with 1×10^4 cells per each well were supplied with standard nutrient medium. After 12 and 24 h of culture, the cells were washed with PBS and stained with the FDA solution.

The solution consists of 30 μl of FDA stock solution (1 mg FDA/ml acetone) diluted in 10 ml PBS. After an incubation period of 15 min at 37 °C in the dark environment, the FDA solution was suctioned off and replaced by 500 μl PI stock solution (1 mg PI/ml distilled water) diluted in 10 ml PBS. After an incubation of 2 min, the cells were washed twice with PBS. Within 1 h after the staining, the cells were examined *via* a fluorescence microscope (Axioplan2) and documented with a digital camera (AxioCam MRc5 from ZEISS, Germany). The dyes could be excited at 488 nm (blue light, argon laser). The green fluorescence (FDA) was detected at 530 nm whereas the red fluorescence (PI) was detected at 620 nm.

2.6. Analysis of cell proliferation

The proliferation of HOBs *in vitro* was measured using MTT and BrdU test following the 12 and 24 hours of incubation according to the manufacturer guidelines. The measurement presented proliferation differences between the Au–TiO_2, TiO_2, and Ti (control) with a statistical significance level of 0.05 at 95% confidence level.

Cell proliferation was assessed by using the MTT Cell Proliferation Kit (#11465007001, Roche Diagnostics, Mannheim, Germany). 96-well microtiter plates with 5×10^3 cells per well were incubated for 12 and 24 hours and a sample of 100 μl eluate was obtained and cell proliferation was measured. The

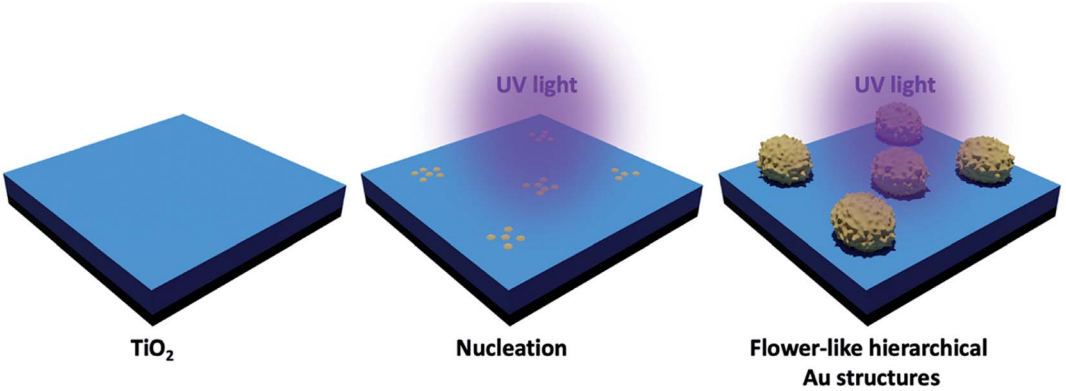

Fig. 1 Schematic representation of the photocatalytic deposition of Au structures on the TiO_2 thin film surface.

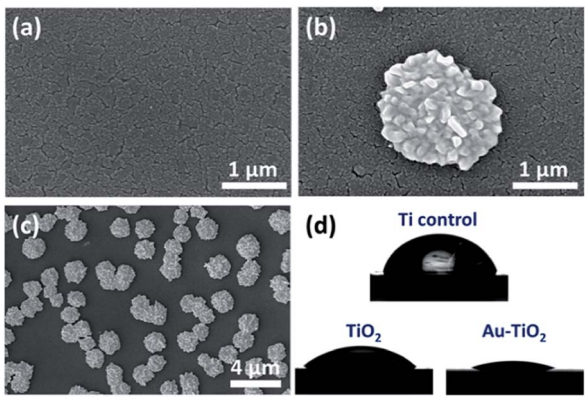

Fig. 2 SEM image of (a) TiO_2 and flower-like hierarchical Au structures modified TiO_2 at (b) high and (c) low magnification. (d) Images for contact angle properties of prepared samples.

optical density of the samples was measured photometrically at 450 nm wavelength.

Proliferating cells were determined by using the BrdU (Bromdesoxyuridin) Cell Proliferation ELISA (enzyme-linked immunoadsorption) kit (Roche Diagnostics, Mannheim, Germany). 96-well microtiter plates with 5×10^3 cells per well were incubated and a sample of 150 μl eluate was obtained. The optical density of the individual samples was measured in a microplate reader (Specta Max plus 384, Molecular Devices, Sunnyvale, USA) at 450 nm wavelength.

2.7. Analysis of cell morphology

Exactly 12 and 24 h after culture on surfaces, SEM was carried out to observe the proliferation characteristics of HOBs. The samples were fixed in 4% glutaraldehyde (Electron Microscopy Sciences, Washington, PA, USA), rinsed with 0.2 M sodium cacodylate buffer, pH 7.4 (Sigma-Aldrich), post-fixed with 1% osmium tetroxide (Sigma-Aldrich), and then rinsed in sodium cacodylate buffer. Thereafter, the cells were immersed in a solution of 1% tannic acid (Sigma-Aldrich) and 0.1 M sodium cacodylate solution for 60 min and rinsed with 0.2 M sodium cacodylate. The samples were dehydrated by crescent alcohol concentrations followed by hexamethyldisiloxane prior to sputter-coating (20 nm gold/palladium) and evaluation by using a Zeiss Sigma FE-SEM microscope (Carl Zeiss Inc.).

2.8. Statistical analysis

The experiments were performed in triplicate, and each result is reported as the mean ± SD. Data between three or more groups were compared using the one-way analysis of variance, followed by Dunnett's post hoc test. $P < 0.05$ was considered to be statistically significant.

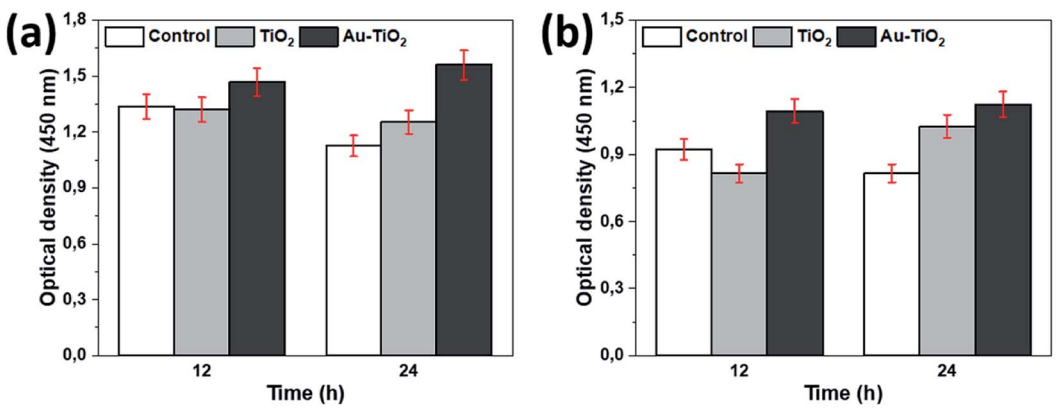

Fig. 3 (a) BrdU and (b) MTT assays.

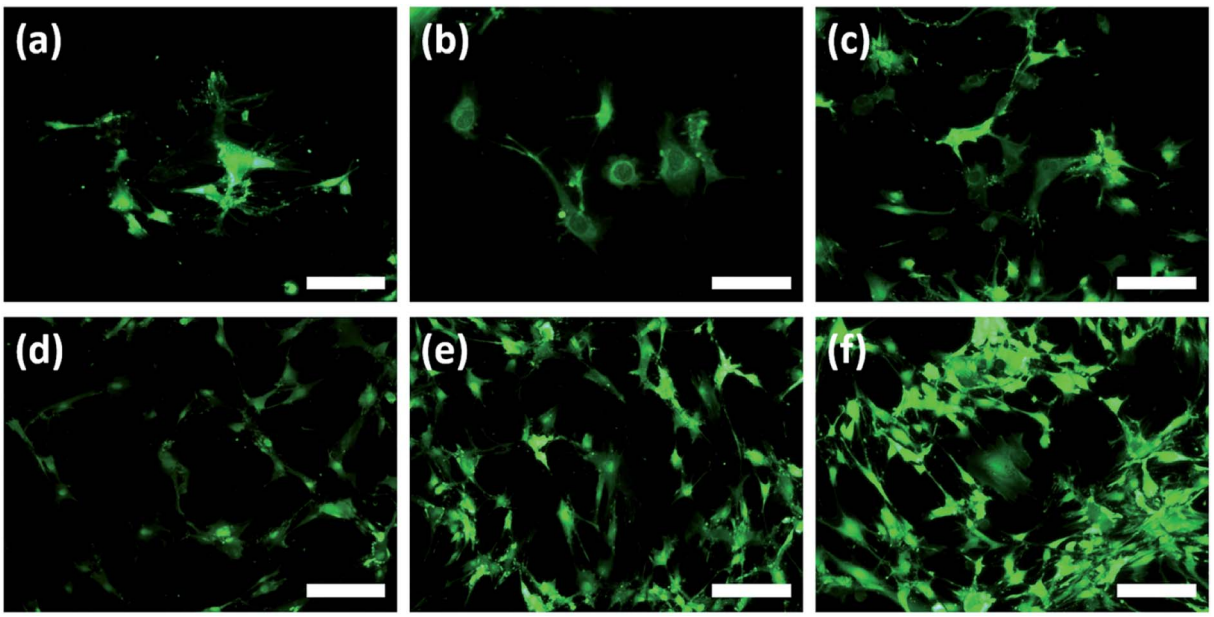

Fig. 4 Fluorescence imaging of HOBs on (a), (d) Ti control, (b), (e) TiO_2 and (c), (f) flower-like hierarchical Au structures modified TiO_2 at 12 h and 24 h culturing time (scale bar: 200 μm) (upper and bottom images represent 12 h and 24 h culturing time, respectively).

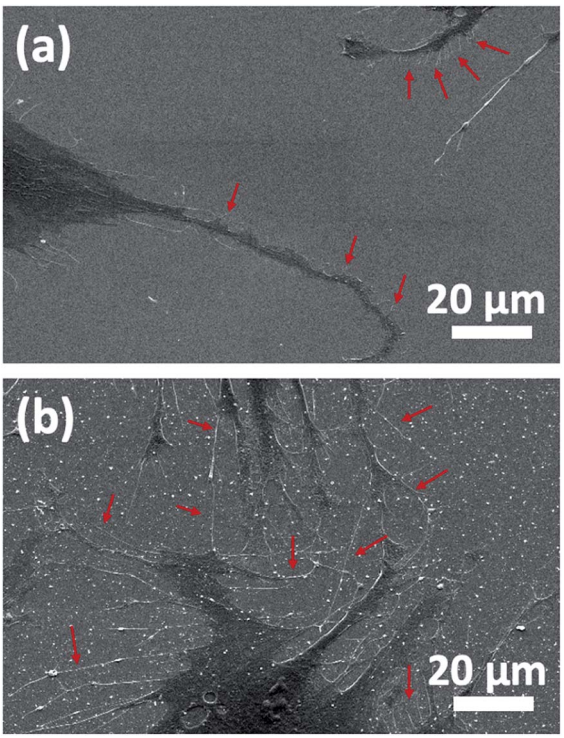

Fig. 5 SEM analysis of HOBs on (a) TiO_2 and (b) Au–TiO_2 surfaces. The trunks of the filopodial extensions prone to converge Au clusters.

3. Results and discussion

As shown in Fig. 2a, TiO_2 thin film exhibits a columnar grain structure, which is typical for sputter-deposited layers. As reported previously, such nanocracks form during the sputtering at high oxygen partial pressure (oxygen oversaturation prevents the formation of a dense contact between adjacent TiO_2 columnar structures).[14,26] After UV illumination, it is obvious that flower-like hierarchical Au structures are uniformly distributed on the nano cracked TiO_2 surface (Fig. 2b). The size of the flower-like hierarchical Au structures are in the range of 2–5 μm (Fig. 2c). At a closer look one can see that these flower-like microstructures are composed of nanoscale protrusions (Fig. 5b). Piling of Au clusters over each other led to a hierarchical ordering which reminds of a pinecone structure.

We observed that the control Ti and TiO_2 deposited substrates exhibited comparable wetting behavior with CAs of $70 \pm 3^\circ$ and $63 \pm 2^\circ$, respectively (Fig. 2d). However, after adding flower-like hierarchical Au structures on TiO_2 layer we observed superwetting with CA $<5^\circ$. The topographic features (combination of micro-and nanostructures) induced by photocatalytic deposition of Au seem to foster the wetting, which is in agreement with Wenzel model. According to the Wenzel model, increasing the roughness of a hydrophilic surface increases its hydrophilicity.[27]

Following the surface analysis, we revealed the cellular response on prepared surfaces by assessing cell metabolic activity and proliferation. MTT and BrdU tests presented significant differences between the prepared and the control surfaces. A higher metabolic activity on Au–TiO_2 surface was observed at both examination times (12 h and 24 h), compared to TiO_2 and Ti surfaces (Fig. 3).

Additionally, Au–TiO_2 was found to induce the highest cell proliferation; although BrdU incorporation in all surfaces has also increased over time. Both TiO_2 and Au–TiO_2 did not show any cytotoxicity since none of them presented lower viability than Ti control. In general, HOBs on TiO_2 and Au–TiO_2 samples presented a higher cell count than Ti control. There is a significant increase in the number of vital cells in all samples over

time. Following 12 h cell-culturing period, FDA/PI analysis revealed regular cell structures in all samples; however, the number of filopodia and membrane protrusions was relatively higher on the Au–TiO_2 surfaces.

According to the 24 h results, an increase of the cell numbers could be seen, however, the Au–TiO_2 surfaces exhibited higher degree of cell-to-cell contact. Overall, HOBs presented a well-spread morphology on all surfaces and formed a nearly complete coverage of surfaces after 24 hours (Fig. 4). Fluorescent imaging showed that HOBs remained viable on all surfaces especially with a higher number of filopodia formation on Au–TiO_2 surfaces (Fig. 4c and f).

The filopodia formation and concomitant cell-to-cell contact were relatively lower on Ti control after 24 h (Fig. 4b and d). However, after 12 h cultivation period we observe that membrane protrusions were short and not branched on both Ti and TiO_2 surfaces. The HOBs cultured on TiO_2 surface exhibited a spherical morphology and there are only a few filopodia without any branching or enlargement (Fig. 4b), whereas HOBs on Ti control exhibited abnormal cell morphologies with irregular cell borders despite weak filopodia-like membrane protrusions (Fig. 4a).

In addition to fluorescence imaging, SEM analysis was performed to determine the cell–surface interactions by clearly displaying the formation of the filopodia and their attachment to the surface features. Morphological findings observed by SEM were in accordance with those detected in the FDA/PI staining. While a limited number of filopodia and cellular protrusion were observed on TiO_2 (arrows show less and short filopodia formation in Fig. 5a), there was a significant orientation of filopodia extensions towards Au clusters on Au–TiO_2 surface, which fostered early cell-to-cell contact formation (Fig. 5b). Densely distributed filopodia could also indicate an efficient adhesion to the Au–TiO_2 surface.[7] Moreover, the trunks of the filopodial extensions prone to converge the Au clusters (arrows indicate such extension in Fig. 5b).

4. Conclusions

The precise role of the surface topography on the early events in implantable orthopedic and dental devices remain poorly understood. In addition, comparative *in vitro* studies with different implant surfaces are rarely performed. Within the limited knowledge current study, it could be concluded that the TiO_2 surface decorated with hierarchical Au structures (composed of both micro- and nanoscale features) stimulates a superior osteoblast organization with elevated filopodias. Thus, the proposed method could offer novel patterning of Ti-based surfaces with different types of metallic (not limited to only Au) structures for medical implantable devices. However, further experimental, and clinical studies are needed to clarify the exact characteristics of this composition.

Conflicts of interest

There are no conflicts to declare.

Acknowledgements

Authors thank to NanoBMT Co. Ltd. for supporting cell viability and proliferation analysis.

References

1 K. M. Hotchkiss, G. B. Reddy, S. L. Hyzy, Z. Schwartz, B. D. Boyan and R. Olivares-Navarrete, *Acta Biomater.*, 2016, **31**, 425–434.
2 A. Bagno and C. Di Bello, *J. Mater. Sci.: Mater. Med.*, 2004, **15**, 935–949.
3 Y. Li, Y. Song, A. Ma and C. Li, *BioMed Res. Int.*, 2019, **2019**, 1–12.
4 X. Liu, S. Chen, J. K. H. Tsoi and J. P. Matinlinna, *Regener. Biomater.*, 2017, **4**, 315–323.
5 Y. Li, B. Li, Y. Song, A. Ma, C. Li, X. Zhang, H. Li, Q. Zhang and K. Zhang, *Dent. Mater. J.*, 2019, **38**, 278–286.
6 M. Veith, O. C. Aktas, W. Metzger, D. Sossong, H. Ullah Wazir, I. Grobelsek, N. Pütz, G. Wennemuth, T. Pohlemann and M. Oberringer, *Biofabrication*, 2010, **2**, 035001.
7 C. Aktas, E. Dörrschuck, C. Schuh, M. M. Miró, J. Lee, N. Pütz, G. Wennemuth, W. Metzger, M. Oberringer, M. Veith and H. Abdul-Khaliq, *Mater. Sci. Eng., C*, 2012, **32**, 1017–1024.
8 Y.-T. Sul, C. Johansson, A. Wennerberg, L.-R. Cho, B.-S. Chang and T. Albrektsson, *Int. J. Oral Maxillofac. Implants*, 2005, **20**, 349–359.
9 E. P. Su, D. F. Justin, C. R. Pratt, V. K. Sarin, V. S. Nguyen, S. Oh and S. Jin, *Bone Joint J.*, 2018, **100B**, 9–16.
10 B. Valdez-Salas, E. Beltrán-Partida, S. Castillo-Uribe, M. Curiel-Álvarez, R. Zlatev, M. Stoytcheva, G. Montero-Alpírez and L. Vargas-Osuna, *Molecules*, 2017, **22**, 832.
11 L. Liu, R. Bhatia and T. Webster, *Int. J. Nanomed.*, 2017, **12**, 8711–8723.
12 Y. Fu and A. Mo, *Nanoscale Res. Lett.*, 2018, **13**, 187.
13 Y. Yang, S. Park, Y. Liu, K. Lee, H. S. Kim, J. T. Koh, X. Meng, K. Kim, H. Ji, X. Wang and J. L. Ong, *Vacuum*, 2008, **83**, 569–574.
14 A. Vahl, S. Veziroglu, B. Henkel, T. Strunskus, O. Polonskyi, O. C. Aktas and F. Faupel, *Materials*, 2019, **12**, 2840.
15 W. Metzger, B. Schwab, M. M. Miro, S. Grad, A. Simpson, M. Veith, G. Wennemuth, V. Zaporojtchenko, S. Verrier, J. S. Hayes, M. Bubel, T. Pohlemann, M. Oberringer and C. Aktas, *J. Biomed. Nanotechnol.*, 2014, **10**, 831–845.
16 P. Pansila, N. Witit-Anun and S. Chaiyakun, *Procedia Eng.*, 2012, **32**, 862–867.
17 S. J. Fonash, *J. Electrochem. Soc.*, 1990, **137**, 3885.
18 S. Veziroglu, M. Z. Ghori, M. Kamp, L. Kienle, H. G. Rubahn, T. Strunskus, J. Fiutowski, J. Adam, F. Faupel and O. C. Aktas, *Adv. Mater. Interfaces*, 2018, **5**, 1800465.
19 J. Wu, Y. Qu, Q. Yu and H. Chen, *Mater. Chem. Front.*, 2018, **2**, 2175–2190.
20 M. F. Cardinal, E. Vander Ende, R. A. Hackler, M. O. McAnally, P. C. Stair, G. C. Schatz and R. P. Van Duyne, *Chem. Soc. Rev.*, 2017, **46**, 3886–3903.

21 M. Takahashi, M. Kikuchi and O. Okuno, *Dent. Mater. J.*, 2004, **23**, 203–210.
22 S. Veziroglu, M. Z. Ghori, A. L. Obermann, K. Röder, O. Polonskyi, T. Strunskus, F. Faupel and O. C. Aktas, *Phys. Status Solidi A*, 2019, **216**, 1–6.
23 M. Z. Ghori, S. Veziroglu, B. Henkel, A. Vahl, O. Polonskyi, T. Strunskus, F. Faupel and O. C. Aktas, *Sol. Energy Mater. Sol. Cells*, 2018, **178**, 170–178.
24 S. Veziroglu, A.-L. Obermann, M. Ullrich, M. Hussain, M. Kamp, L. Kienle, T. Leißner, H.-G. Rubahn, O. Polonskyi, T. Strunskus, J. Fiutowski, M. Es-Souni, J. Adam, F. Faupel and O. C. Aktas, *ACS Appl. Mater. Interfaces*, 2020, **12**, 14983–14992.
25 S. Veziroglu, M. Ullrich, M. Hussain, J. Drewes, J. Shondo, T. Strunskus, J. Adam, F. Faupel and O. C. Aktas, *Surf. Coat. Technol.*, 2020, **389**, 125613.
26 A. Vahl, J. Dittmann, J. Jetter, S. Veziroglu, S. Shree, N. Ababii, O. Lupan, O. C. Aktas, T. Strunskus, E. Quandt, R. Adelung, S. K. Sharma and F. Faupel, *Nanotechnology*, 2019, **30**, 235603.
27 R. Rosario, D. Gust, A. A. Garcia, M. Hayes, J. L. Taraci, T. Clement, J. W. Dailey and S. T. Picraux, *J. Phys. Chem. B*, 2004, **108**, 12640–12642.